ChemComm

COMMUNICATION

View Article Online
View Journal | View Issue

Cite this: *Chem. Commun.*, 2018, **54**, 9305

Received 18th May 2018,
Accepted 26th July 2018

DOI: 10.1039/c8cc03986k

rsc.li/chemcomm

Chemistry of 4-[(4-bromophenyl)ethynyl]pyridine at metal surfaces studied by STM†

Jindong Ren,[ab] Eugene Larkin,[c] Colm Delaney,[c] Yang Song,[d] Xin Jin,[d] Saeed Amirjalayer,[ab] Anne Bakker,[ab] Shixuan Du,[d] Hongying Gao,*[ab] Yu-Yang Zhang,*[d] Sylvia M. Draper*[c] and Harald Fuchs*[ab]

Molecular architectures (Kagome networks, coordinated/covalent dimers and branched coordination chains) *via* self-assembly, Ullmann reaction and pyridine coordination of 4-[(4-bromophenyl)ethynyl]-pyridine are found to be sensitive to the underlying metallic surfaces. The molecular species were characterised on the surface by low-temperature scanning tunnelling microscopy (LT-STM) at sub-molecular level.

An understanding of heterogeneous catalysis at the sub-nanometer scale is important, both for investigating surface reaction mechanisms and building advanced molecular devices.[1] Versatility in the synthesis of complex architectures requires the control of the on-surface reactivity[2] and metal-directed self-assembly.[3] The Ullmann reaction,[4] a well-known organic reaction mediated by metal catalysts, has been used to link aromatic units through C–C bonds and to further construct regular chains or complex porous networks. Furthermore, noble metal atoms involved in coordination and adatom bonds also take-on specific roles in building supramolecular quasicrystalline materials.[5] The judicious choice and application of these various types of reactivity, therefore, offer opportunities for the formation of organic frameworks with targeted applications in future molecular devices.[6]

Here, we have investigated the self-assembly, Ullmann reaction and pyridine coordination of 4-[(4-bromophenyl)ethynyl]pyridine (44BEP) on sublimation under ultrahigh vacuum onto various crystalline metallic surfaces and in line with density-functional-theory (DFT) calculations.[7] Recently, Shen *et al.*[8] reported on the hierarchical formation of N–metal–N and C–metal–C coordination modes on metallic surfaces by using 5-(2-(4-bromophenyl)-ethynyl)pyrimidine (BPPA). Given that the on-surface chemistry of these species revolves around the reactivity of the N-atoms of the pyrimidine ring, the pyridine molecule is expected to show different self-assembly behaviours as well as subsequent coordination/covalent chemistry (Scheme S1, ESI†). The origin is a subtle balance between the distances from the substrate to the N- and Br-atoms respectively, which is dependent on the type of metal substrate (Scheme 1). Synthetic procedure and NMR Spectra for 44BEP are listed in the ESI.† Au(111), Ag(111) and Cu(111) were chosen to study the roles played by the metallic catalysts in surface chemistry. All STM images were acquired with the same parameter ($I = -0.1$ nA, $V_b = -2.0$ V). Similar to Björk *et al.*,[9] DFT calculations (Table S4, ESI†) focusing on the interaction between 44BEP and various metal surfaces demonstrate that the different distances between two side groups (pyridine N and bromide) and substrates will cause different self-assembly behaviours and chemical reactions. In contrast to the disordered networks on Au(111), self-assembly architectures of closely stacked Kagome lattices were observed on the Ag(111) surface at room temperature. Ullmann reaction intermediates in two different phases were found on the Ag(111) substrate after thermal annealing. Novel branched coordinated chains were identified on the Cu(111) surface. These observations demonstrate the decisive catalytic role played by the metal atoms in surface assembly behaviour and in the following chemical reactions of the 44BEP molecule.

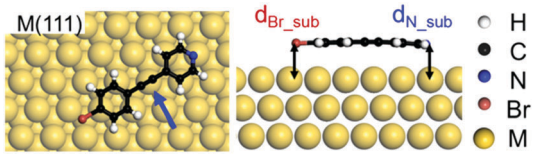

Scheme 1 Schematic diagram of the DFT optimized orientation of 44BEP on metal (M) surfaces. The different distances (d_{Br_sub} and d_{N_sub}) on different surfaces will bring different configurations and self-assembling behaviours.

[a] *Physikalisches Institut, Westfälische Wilhelms-Universität, Wilhelm-Klemm-Straße 10, 48149 Münster, Germany. E-mail: gaoh@uni-muenster.de, fuchsh@uni-muenster.de*
[b] *Center for Nanotechnology, Heisenbergstraße 11, 48149 Münster, Germany*
[c] *School of Chemistry, Trinity College Dublin, The University of Dublin, Dublin 2, Ireland. E-mail: smdraper@tcd.ie*
[d] *Institute of Physics, University of Chinese Academy of Sciences, Chinese Academy of Sciences, Beijing 100190, P. R. China. E-mail: zhangyuyang@ucas.ac.cn*

† Electronic supplementary information (ESI) available: Synthetic procedure, related NMR spectra, STM related measurements and DFT calculations. See DOI: 10.1039/c8cc03986k

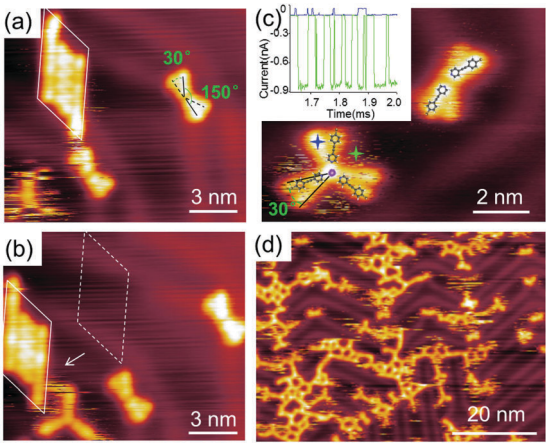

Fig. 1 STM images of 44BEP on Au(111). (a and b) Show subsequent images of the same scanning area of a low-coverage sample where the island's position has changed. (c) Close-up image of the dimer and trimer on Au(111). Brightness contrast of the lobes and I–t spectra (inset, 0.1 nA, −2.0 V.) show the swing of the dimer and the rotation of the trimer. The purple sphere in the centre of the trimer is an additional Au adatom. The vibration angles (30° and 150°) are shown in (a). (d) At high coverage, the dimers and trimers are connected to form disordered networks.

Fig. 1 displays a series of images of Au(111) surfaces with a low coverage of molecules scanned at 77 K. The molecules are seen to self-assemble into several structures after adsorbing onto the substrate.[10] The STM tip could be used to move the densely packed islands of intact molecules, thus indicating a weak coupling between Au(111) surface and molecules. Dimers and trimers are the main constructions on the surface and act as nuclear seeds for the growth of the larger molecular networks. The dimer, appearing as four lobes due to its swinging motion at 77 K, only adsorbs at the elbow sites of the Au(111) herringbone template. Each dimer is constructed by two 44BEP molecules connected through a 150° angle. The dimer can swing between two stable sites at 30° from the focal point, leading to the observed four lobes in the STM image, see Fig. 1a. The stable sites are determined by the underlying symmetric arrangement of Au atoms. As for the trimer, the central bright sphere indicates an additional Au atom is present. Furthermore, the molecular orientations inferred from the models presented in Fig. 1c suggest that there is N–Au coupling in the trimer.

To prove the postulated swing and rotation behaviours, I–t spectra[11–14] were performed. As reported, Stipe *et al.* demonstrated the direct monitoring of single molecular motion by recording the tunnelling current as a function of time.[15] After placing the STM tip above a certain pre-selected position, the feedback loop is switched off, leading to a fixed tip height in the succeeding measurements. Dynamical behaviours such as molecular motion under the tip will lead to an abrupt change in the tunnelling current. Fig. 1c (inset) displays the spectra detected above and between the lobes indicated in Fig. 1c. Taking the blue spectrum as an example, the measured absolute value of the current is high when first fixing the tip upon molecule. Since the rotation of the molecule moves the molecular lobe out of the tunnelling gap, it results in a larger tunnelling gap distance and lower tunnelling current (absolute value) between the tip and sample. The tunnelling current reverts back to a high value when the rotation moves the molecule back into the tunnelling gap. Similarly, for the green spectrum, when the molecular lobe rotates into the tunnelling gap, a much higher tunnelling current is detected. Therefore, the high and low current states correspond to the molecular lobes moving inside and outside of the tunnelling junction, and demonstrate the rotation of the molecules. By checking the calculated $d_{\mathrm{Br\_sub}}$ and $d_{\mathrm{N\_sub}}$ (see Table S4, ESI†), we found that there is no chemical bond between 44BEP and Au(111). The largest binding energy is 1.85 eV. It is also found that the energy difference between different binding sites is very small[16] (less than 0.1 eV), indicating a small diffusion and rotation barrier, which explains the fast rotation of 44BEP molecules. Details of the DFT calculations can be found in the ESI.†

Further deposition of the molecules on the Au(111) surface gives rise to disordered networks that nucleate around the existing dimers and trimers, see Fig. 1d. The swing and the rotation of the molecules are hindered by increasing proximity of neighbouring molecules. Unlike the regular and robust structures observed on the Ag(111) and Cu(111) crystals, the networks generated on the Au(111) surface are easily removed by the STM tip demonstrating that they are weakly coupled to the Au(111) surface. Gradual annealing of the sample leads only to the desorption of molecules from the Au(111) surface.

To determine the role of the supporting substrate in the chemical reactivity, we changed the crystalline substrate to Ag(111). After evaporation of ~0.5 ML 44BEP molecules onto Ag(111) at 300 K, a regular Kagome lattice[17] was formed. The typical size of the unit length in the Kagome networks is 5.00 ± 0.05 nm. Fig. 2a displays a high resolution image of the Kagome lattice super-imposed by the optimized molecular model. Each 44BEP molecule is imaged as an assembly of

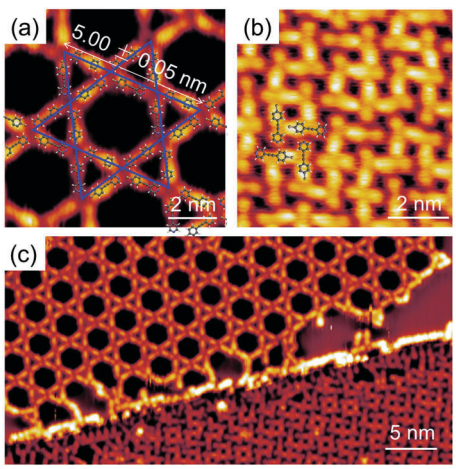

Fig. 2 STM images of self-assembled molecules on a Ag(111) surface. (a) The delicate interaction between the Br and H leads to the formation of a Kagome lattice at low coverage. (b) The close packed structure found on increasing the molecular coverage. (c) Coexistence of Kagome lattice and close-packed layer in large scale STM image.

bright ellipsoids and dim spheres. The combination of the Br atom and the benzene ring enhances the topography intensity and results in the bright protrusion observed.

It is easy to discern from the images that each four-branch joint in the Kagome lattice contains two Br ended branches and two pyridine N ended branches. The Br terminated branches are arranged in a straight line while a displacement of 0.42 ± 0.05 nm is observed for the N terminated parallel branches. Although the molecules are not connected to each other at 77 K, the lattice is stabilized by some Br···H–C hydrogen bonds indicated by the molecular modelling. The distance between the Br and the nearest H is 0.28 ± 0.05 nm, which is reasonable for hydrogen bonds.[18]

Fig. 2c demonstrates both a porous Kagome lattice and a close-packed molecular layer. Due to the Br protrusion in 44BEP molecule, there is a large displacement between each molecules and its closest molecule and the delicate Br···H–C interaction is disturbed, to give a quasi-regular structure at high coverage, see Fig. 2b. This is different from the BPPA tetramers held by C–H···N hydrogen bonds.[19] DFT calculations show that by forming this quasi-regular structure with Br···H–C, the binding energy of one 44BEP molecule on a Ag(111) substrate increased from 1.72 eV to 1.97 eV per molecule. Furthermore, desorption of the molecule leads to the appearance of a Kagome lattice for the high coverage sample if the sample is held at 380 K for 10 min.

To investigate the possibility of on-surface coupling reactions, we annealed the sample gradually and observed two different phases of the intermediate caused by an Ullmann reaction around 410 K (see Fig. 3a and c). Here, the 44BEP molecules are completely debrominated by the Ag surface, resulting in such Ag-bridged organometallic intermediates. The length of the main uniform bars which are constructed by one Ag adatom and two molecules is 2.20 ± 0.05 nm. The Ag atoms are either extracted from the terraces or originated from the free Ag gas on the surface during the previous annealing process.[4] As for the intermediates, the Ag adatom can be easily distinguished in the middle of the bars. The split-off Br adatoms, also appear as spheres between the bars. We labelled the bars according to their different orientations, as a parallel (Fig. 3a) or a chevron phase (Fig. 3c). Further high-resolution images are presented in Fig. 3b and d. These provided sub-molecular resolution images of the two phases, and enabled us to construct molecular models. The spherical protrusion in the centre of the dimer can be easily discerned and is attributed to a single Ag adatom based on previously published results.[4,20]

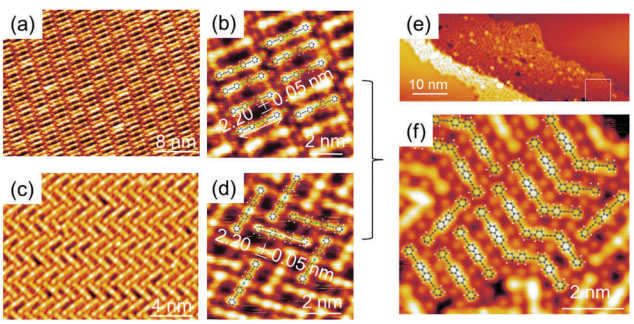

Fig. 3 STM topography images of the densely packed molecular layer on a Ag(111) surface at different stages during the annealing process. (a–d) Two different phases (described as parallel (a) and (b) and chevron phases (c) and (d)) of the organometallic dimers were found after annealing sample to 410 K. (e and f) Both Ullmann reaction and N induced activation give rise to the formation of chain structures after annealing.

In the case of the parallel phase, each bar is terminated by one Ag adatom, which is observed as a sphere at the end of the bar. For the chevron phase, the central Ag adatom appears brighter with respect to the molecule and there is no sphere attached at the end. We attributed this contrasting modulation, *i.e.* dim and bright centres for the Ag adatoms, to the different adsorption configurations in relation to the surface. For the parallel phase with the Ag adatom at each termination, the central Ag adatom will be lifted by the linked molecules. Thus, the vertical displacement with respect to the substrate will cause a poor conduction during STM scanning and result in a dimmer feature in the centre of the bars.

On further annealing the sample to 480 K for 10 min, the release of the coordinating Ag atoms in C–Ag–C bonds induces covalent C–C coupling between the aromatic species.[21] The remaining adjacent benzene rings twist and are no longer parallel with respect to the substrate surface. They are therefore imaged as two bright protrusions in the new bar centre. The C–H bonds adjacent to the N atom in the pyridine ring are activated and form a covalent bond with the Ullmann free radical of another 44BEP molecule, leading to the formation of some short zigzag chains on the surface, see Fig. 3e and f. Due to desorption of the molecule during annealing, these products mainly assemble at the step edge sites.

We also took measurements on a Cu(111) crystal which is more active than Au(111) and Ag(111). Our calculations also show that 44BEP has a larger binding energy on Cu(111). Fig. 4a depicts a large-scale STM image of a Cu(111) surface covered by one dimensional (1D) chains after depositing the molecules at 300 K.[22] The chains show a preference for 1D growth with three-branch junctions at high coverage. To probe the specific sites of the complexation in each chain, a high-resolution image with dim-bright contrast is shown in Fig. 4b and superimposed with the fitted molecular structures. The repeating unit of 1.20 ± 0.05 nm unit length, corresponds to one 44BEP molecule. The higher intensity observed here is attributed to the Br atom. This is helpful to the identification of the molecular position in the chain. The molecular orientation at each site in the chain is either parallel or antiparallel with respect to the neighbouring molecules. This results in three different dimer configurations, *i.e.* Br–Br, Br–N and N–Cu–N (see Fig. 4c) after considering the measured centre-to-centre distances. As for the last N–Cu–N connection, it is well known that Cu adatoms form a two-dimensional gas on the surface during the annealing process.[4] The reactive Cu adatom can then participate in the formation of an organometallic chain and cause the dim sphere apparent between each N–N connection. This is apparent from the high-resolution images and the lateral distance measurements in Fig. 4c. Indeed, each molecule in the dimer is stabilized by hydrogen bonding or N–Cu–N coupling. A statistical analysis of the dimer in the chain, based on several hundreds of connections obtained from STM images (10 nm × 10 nm), determined

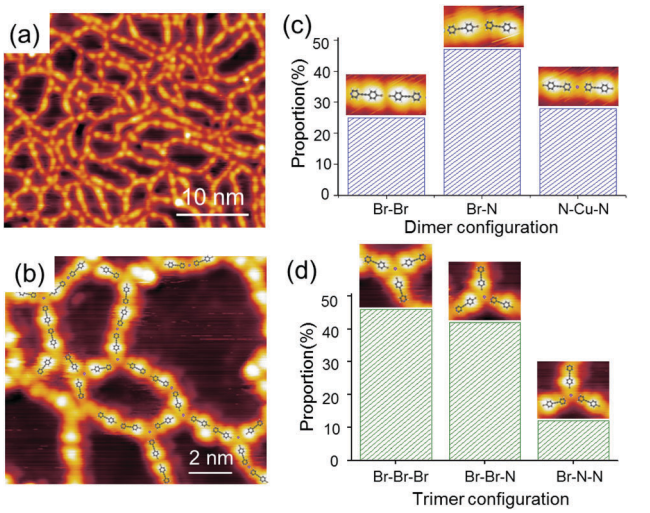

Fig. 4 STM topography images of molecules on the Cu(111) surface. (a and b) Organometallic chains were found after depositing molecule at room temperature. (c and d) Statistic of each configurations of dimer (c) and trimer (d) in the chain on Cu(111) surface. The purple ball represents the Cu atom.

that the ratios of the Br–Br, Br–N and N–Cu–N connections are 25%, 47% and 28% respectively (Fig. 4c). The random nature of the connections demonstrates that the Br and N atoms in the molecule play a similar role in the 1D chain formation.

For the three-branch junctions (Fig. 4d), only three types of junction, classified by the number of Br terminated branches, were found on the surface. In fact, no three-branch junctions originated from three N terminated branches in our experiment. The proportions of the three-branch junctions involving three, two or one Br atoms were 46%, 42% and 12% respectively. The high ratios of the three and two Br type junctions, probably indicates the preferential formation of the three-branch junction at Br–Br sites when two chains touch each other at high coverage. Furthermore, a dim sphere attributed to a Cu adatom appears in the centre of every three-branch junction. This suggests that a Cu adatom is critical to the construction of such junctions in the molecular networks. We also gradually annealed the sample. Neither regular C–Cu–C organometallic products nor covalent dimer products were observed on the Cu(111) surface.

In conclusion we have demonstrated both the self-assembly and dehalogenation of 44BEP molecules on different crystal surfaces at sub-molecular level. We have shown that the molecular architectures formed are sensitive to the underlying crystalline metal surfaces due to distance-induced effects. This reveals the important role of noble metal species in the construction of large scale regular molecular lattices and in catalysing the C–Br bond dissociation. For Au(111), both swinging and rotational motions of the dimer and trimer indicate a high mobility and weak surface coupling with the surface. Kagome lattices stabilized by Br···H–C and N···H–C hydrogen bonds are produced on Ag(111) surfaces resulting in regular self-assembled architectures. C–C bonds formed by Ullmann reactions and pyridine induced C–H activations, reveal a way to potentially build large scale chains in a controlled manner. While for the Cu(111) surface, the random connection between two neighbouring molecules in linear chains and selective three-branch junctions at Br···Br sites offer opportunities to design tailored molecular architectures. These results shed new light on how to fabricate supramolecular devices using a bottom-up approach.

The authors acknowledge financial support from the Deutsche Forschungsgemeinschaft (SFB 858, TRR 61, GA 2430/1-1, AM 460/2-1), Science Foundation Ireland (SFI 14/IA/3046, SFI 15/IACA/3413), CAS Pioneer Hundred Talents Program and Beijing Nova Program (No. Z181100006218023).

Conflicts of interest

There are no conflicts to declare.

Notes and references

1 Y.-Q. Zhang, M. Paszkiewicz, P. Du, L. Zhang, T. Lin, Z. Chen, S. Klyatskaya, M. Ruben, A. P. Seitsonen, J. V. Barth and F. Klappenberger, *Nat. Chem.*, 2018, **10**, 2924.
2 H. Kong, S. Yang, H. Gao, A. Timmer, J. P. Hill, O. Diaz Arado, H. Monig, X. Huang, Q. Tang, Q. Ji, W. Liu and H. Fuchs, *J. Am. Chem. Soc.*, 2017, **139**, 3669–3675.
3 A. Dmitriev, H. Spillmann, N. Lin, J. V. Barth and K. Kern, *Angew. Chem., Int. Ed.*, 2003, **42**, 2670–2673.
4 W. Wang, X. Shi, S. Wang, M. A. Van Hove and N. Lin, *J. Am. Chem. Soc.*, 2011, **133**, 13264–13267.
5 M. Knor, H. Y. Gao, S. Amirjalayer, A. Studer, H. Gao, S. Du and H. Fuchs, *Chem. Commun.*, 2015, **51**, 10854–10857.
6 X. Zhang, N. Li, H. Wang, C. Yuan, G. Gu, Y. Zhang, D. Nieckarz, P. Szabelski, S. Hou, B. K. Teo and Y. Wang, *ACS Nano*, 2017, **11**, 8511–8518.
7 R. Gutzler, H. Walch, G. Eder, S. Kloft, W. M. Heckl and M. Lackinger, *Chem. Commun.*, 2009, 4456–4458.
8 Q. Shen, E. J. Larkin, C. Delaney, Y. Cheng, C. Miao, X. Zhou, L. Liu, W. Huang, H. Gao, S. M. Draper and H. Fuchs, *J. Phys. Chem. C*, 2018, **122**(16), 8954.
9 J. Björk, F. Hanke and S. Stafstrom, *J. Am. Chem. Soc.*, 2013, **135**, 5768–5775.
10 T. A. Pham, F. Song, M. T. Nguyen and M. Stohr, *Chem. Commun.*, 2014, **50**, 14089–14092.
11 T. Kudernac, N. Ruangsupapichat, M. Parschau, B. Macia, N. Katsonis, S. R. Harutyunyan, K. H. Ernst and B. L. Feringa, *Nature*, 2011, **479**, 208–211.
12 Y. Zhang, H. Kersell, R. Stefak, J. Echeverria, V. Iancu, U. G. Perera, Y. Li, A. Deshpande, K. F. Braun, C. Joachim, G. Rapenne and S. W. Hla, *Nat. Nanotechnol.*, 2016, **11**, 706–712.
13 U. G. Perera, F. Ample, H. Kersell, Y. Zhang, G. Vives, J. Echeverria, M. Grisolia, G. Rapenne, C. Joachim and S. W. Hla, *Nat. Nanotechnol.*, 2013, **8**, 46–51.
14 T. Jasper-Toennies, M. Gruber, S. Karan, H. Jacob, F. Tuczek and R. Berndt, *Nano Lett.*, 2017, **17**, 6613–6619.
15 B. C. Stipe, M. A. Rezaei and W. Ho, *Science*, 1998, **279**, 1907–1909.
16 N. Jiang, Y. Y. Zhang, Q. Liu, Z. H. Cheng, Z. T. Deng, S. X. Du, H. J. Gao, M. J. Beck and S. T. Pantelides, *Nano Lett.*, 2010, **10**, 1184–1188.
17 J. Mao, H. Zhang, Y. Jiang, Y. Pan, M. Gao, W. Xiao and H. J. Gao, *J. Am. Chem. Soc.*, 2009, **131**, 14136–14137.
18 J. V. Barth, *Annu. Rev. Phys. Chem.*, 2007, **58**, 375–407.
19 S. K. Hämäläinen, N. van der Heijden, J. van der Lit, S. den Hartog, P. Liljeroth and I. Swart, *Phys. Rev. Lett.*, 2014, **113**, 186102.
20 X. Zhou, C. G. Wang, Y. J. Zhang, F. Cheng, Y. He, Q. Shen, J. Shang, X. Shao, W. Ji, W. Chen, G. Q. Xu and K. Wu, *Angew. Chem., Int. Ed.*, 2017, **56**, 12852–12856.
21 Q. T. Fan, C. C. Wang, Y. Han, J. F. Zhu, J. Kuttner, G. Hilt and J. M. Gottfried, *ACS Nano*, 2014, **8**, 709–718.
22 H. Y. Gao, P. A. Held, M. Knor, C. Muck-Lichtenfeld, J. Neugebauer, A. Studer and H. Fuchs, *J. Am. Chem. Soc.*, 2014, **136**, 9658–9663.

